Int J Adv Manuf Technol (2015) 81:411–421
DOI 10.1007/s00170-015-7185-0

ORIGINAL ARTICLE

Filling holes in digitized point cloud using a morphing-based approach to preserve volume characteristics

Yann Quinsat[1] **· Claire lartigue**[1]

Received: 9 December 2014 / Accepted: 19 April 2015 / Published online: 9 May 2015

Abstract Filling holes is a major challenge to reduce digitizing time and makes the digitized model compatible with applications such as finite element (FE) analysis or inertia calculations. Indeed, whatever the sensor used, for accessibility reasons or reflection problems, some parts of the object may be non-measured defining digitizing holes in the digitized point cloud. In this paper, a method based on a mesh deformation is proposed to fill the digitized holes. The proposed method relies on the a priori knowledge of the numerical model as a nominal mesh. After identifying the digitized holes and calculating the differences between the nominal mesh and the point cloud, a deformation of the nominal mesh is performed. This deformation is determined by minimizing the energy of deformation of the mesh considered as a lattice. The proposed method is validated on a complex shape. Finally, this method is applied to an industrial part in order to highlight interest for balancing issues.

Keywords Digitalization · Energy minimisation · Holes filling · Shape preservation

1 Introduction

Various types of digitizing systems exist to acquire the shapes of a 3D object. Whatever the sensor used, laser plane, structured light or stereo-vision, optical systems allow the acquisition of a great amount of points representative of the part surfaces in a very short time. Researches now focus on using optical measuring systems for in-line production measurements for which measuring time is a critical issue. However, it is commonly admitted that digitized point clouds are noisy, dense, and heterogeneous [14], and that for accessibility reasons or reflection problems, some parts of the object may be non-measured defining digitizing holes in the point cloud Fig. 1. Holes in the object representation could make further applications, such as rapid prototyping [7], Finite element analysis (FEA), or volume calculations difficult to achieve [21, 26]. These holes also contribute to increase the freeform surfaces reconstruction time, which is already a time-consuming operation [2]. Numerous studies [6, 13, 14, 18] deal with the definition of automated measuring strategies with the objective of time minimization while increasing the point cloud completeness, but re-digitizing is generally time-consuming and sometimes incompatible with in-process measurements. Furthermore, some zones could remain inaccessible. Some authors propose to reach the complete 3D object representation by filling the holes [15, 21]. Because of the variety of hole types, a large number of hole-filling algorithms exist, each one more or less dedicated to one specific type [20].

In this study, we use the a priori knowledge of the CAD model of the object under study to overcome the digitizing defects. The algorithm relies on a stress-strain deformation of the nominal geometry performed with the aim of minimizing the differences between the CAD model geometry and the point cloud while preserving the initial topology. It will thus be possible to fill the holes with the deformed geometry. This approach is interesting as it preserves the quality of the identified geometrical characteristics and of the measured dimensions of the object. It is appropriated

✉ Yann Quinsat
yann.quinsat@lurpa.ens-cachan.fr

[1] LURPA, ENS Cachan, Universiteé Paris-Sud,
61 avenue du président Wilson,
F94235 Cachan, France

when the point exploitation requires a complete representation of the object as for FEA, or volume calculation as it is the case in the present paper. In fact, the approach is applied to inertia calculation, first step in crankshaft balancing. As crankshafts are complex parts, some surfaces are difficult to measured, and the digitizing process generally leads to incomplete point cloud presenting digitizing holes. Inertia calculation can only be performed if the discrete data structure is closed. This is performed by filling the holes using the morphing-based approach.

1.1 Related works

Methods for hole-filling generally consist of two subproblems: hole detection and reconstruction of the missing regions [19]. The method proposed by Wang and Oliveira is well-adapted to scanned data. First, a mesh is associated to the point cloud. The boundaries of the holes are detected by identifying the boundary edges (edge belonging to only one triangle). A ring of points around the boundary, defining the boundary vicinity, is used to interpolate the missing portion using a Moving Least Squares procedure. Reconstructed patches preserve and smoothly blend with the original model.

Jun [9] bases his approach on the simple principle that a hole can be filled with planar triangulation (such as Delaunay triangulation) if all the boundary edges are projected onto a plane without auto-intersections. As this only works well for simple holes, complex holes are divided into several simple sub-holes that can be filled using the aforementioned method. In a final step, smoothing is applied to refine the model quality. Li et al. [12] propose to first identify feature curves, then use curve blending to complete the missing parts of the feature curves in the holes. A Bézier-Lagrange hybrid patch relying on the feature curve is then constructed to fill the holes. The method preserves the features but is not completely automated. In their approach, Wang et al. [21] define a method well-adapted to restoring missing curves and corners. Missing feature curves (sharp edges) are reconstructed as B-spline curves. Missing corners are found by minimizing the square of the tetrahedron's volume reconstructed from the potential corner and its neighbors. Holes are thus filled using advancing front method. This method is less adapted to complex surfaces. Wang and Hung [20] propose a method based on Grey System Theory to achieve a smooth and continuous hole filling. Grey system theory is used to reduce randomness and increase regularity in the data. A prediction model is used to identify the location of the future element. In their approach, authors consider two prediction models: the normal vector prediction and the angle prediction. Once newly points are added, a final smoothing stage is performed but curvature is not controlled. Some authors take advantage of 2D images that have been acquired during the measurement stage to recover the missing zones [15, 17]. The 2D images are used as a set of constraints, and as input of a mesh deformation process which tends to minimize the curvature evolution between the inserted facets and the initial mesh. The mesh deformation relies on a mechanical approach for which the mesh is considered as a bar network. With such an approach, that combines techniques of shape from shading and mesh deformation, the overall shape of the part is preserved. However, it requires the use of two measuring systems at the same time. Some authors use morphing to reconstruct missing data with a specific application in dental surface reconstruction. The objective is to align a scanned tooth to a standard model. The approach begins with a one-to-one mapping of feature points of the standard tooth and the scanned tooth thanks to a radial basis function to define the relations for all points in both teeth. A global deformation (translation, rotation, and scaling) is performed followed by local adjustments to align the tooth in preparation to the standard one [23]. In this method, the use of morphing permits to fill the holes by taking advantages of the prior knowledge of the general tooth shape. Morphing is more used in computer graphics for mesh deformation. Two main kinds of approaches exist: the geometric methods and the physically based methods [24]. As far as geometric methods are concerned, lattice or mesh nodes are moved according to geometric constraints to achieve the deformation. In [8], the objective is to relate a template to a target geometry considering some reference points referred to as landmarks. After a general alignment of the landmarks, using translation, rotation, and scaling, the morphing is performed using the landmarks as constraints. The motion of the mesh nodes is interpolated from the motion of the landmarks based on a radial basis function regression to preserve smoothness. The

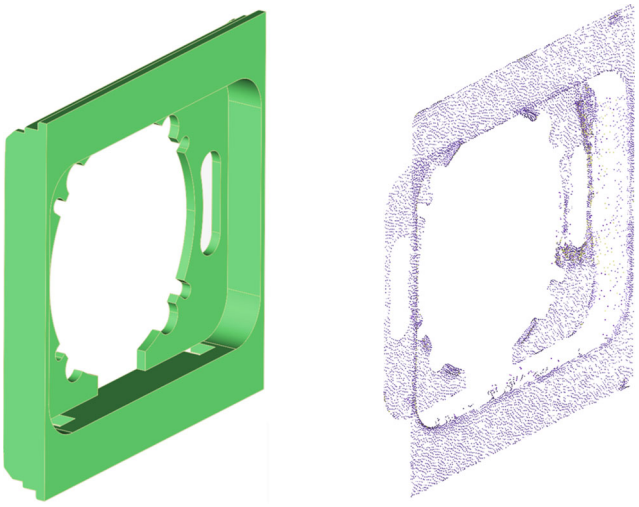

Fig. 1 Digitized holes

method is applied for human-femur reconstruction. In some cases, the morphing can be restrained to a region of interest while preserving the general shape. Kho and Garland [10] propose an iterative sketch-based deformation. The user draws a reference curve in a zone of interest and a second target curve. The deformation is achieved by deforming the reference curve toward the target one. These methods are generally more suited to visualization and animation.

Physically based approaches lead to more realistic results as they rely on energy minimization [5, 15, 17, 24]. As for geometric methods, the 3D object is represented as a triangular mesh, but the deformation is made here considering mechanical energy. Most methods only consider the stretching energy which accounts for length changes and add constraints to preserve the curvature evolution. In our approach, all types of mechanical energy are taken into account: stretching, bending, and torsion energy. Stretching corresponds to length changes, while bending and torsion ensure the overall shape preservation and continuity in curvature evolution.

1.2 Method overview

In this study, the proposed method for hole-filling considers the deformation of the object's CAD model to best approximate the scanned data. The CAD model is represented as a triangular mesh (STL format) (Fig. 2), for which $\{N\}$ is the set of nodes and $\{P\}$ the set of beams defining the triangular facets of the mesh. The mesh deformation is performed according to a physically-based approach based on energy minimization. To preserve curvature continuity, all types of solicitations are considered here: torsion, bending, and stretching.

The big picture of the method proposed to deform the mesh of the nominal part toward the measured data is displayed in Fig. 3. First, a registration step is required to globally align the mesh onto the scanned data. Indeed, to identify holes and perform a deformation that preserves the part shape, a good match between the measured and the nominal features is necessary. To make this registration, numerous methods exist [4, 22, 25], more generally

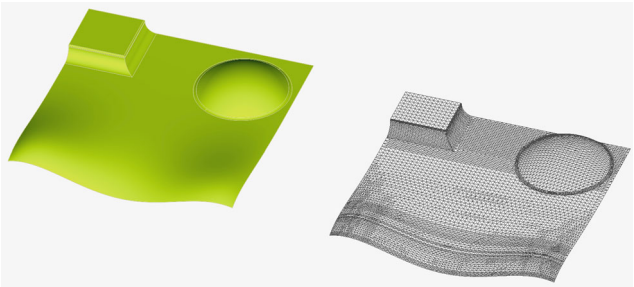

Fig. 2 Surface modeling

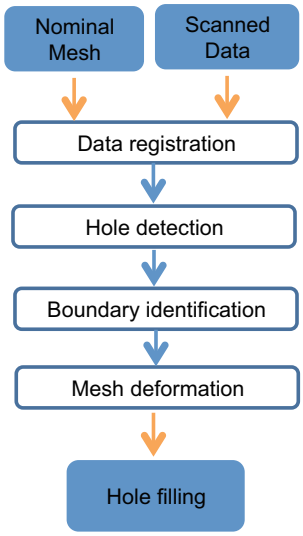

Fig. 3 Proposed approach

based on the well-known ICP algorithm [3]. In the present study, the HT-ICP algorithm is adopted. The second and the third steps focus on hole detection and boundary identification. Indeed, boundaries limit the zones for which the deformation will be performed. The last step is the mesh deformation based on stress-strain energy minimization. The energy minimization relies on a mechanical modeling which is detailed in the next section.

2 Mechanical modeling for energy minimization

The CAD model is represented as a triangular mesh. Each edge defining a facet is considered as a cylindrical beam which is characterized by its length L and its circular section S. The mechanical characteristics are defined by (E, G, I, Io), respectively, the Young's modulus, the torsional modulus, the second moment, and the polar second moment (Table 1).

2.1 Settings

Let us consider the set of m beams $\{P^k\}_{[1,m]}$ and the set of n nodes $\{N_i\}_{[1,n]}$ defining beam's extremities. The displacement of each node is defined by six components, three accounting for the translation (u_i, v_i, w_i) and three

Table 1 Degree of freedom (DOF) description

	DOF	Characteristics
Tension	u	$E.S$
Torsion	α	$G.Io$
Bending in plane (X,Y)	v et β	$E.I$
Bending in plane (X,Z)	w et γ	$E.I$

others for the rotation $(\alpha_i, \beta_i, \gamma_i)$. Data can be expressed in the global frame $\mathcal{R}$ as well as in the local frame $\mathcal{R}^k$ associated to the beam k (Fig. 4). Hence, the following parameters can be defined:

- U_i^k : Node i displacement in the local frame $\mathcal{R}^k$.

$$U_i^k = \left[u_i^k \; v_i^k \; w_i^k \; \alpha_i^k \; \beta_i^k \; \gamma_i^k\right]^t_{\mathcal{R}^k}. \quad (1)$$

- U_i : Node i displacement in the global frame $\mathcal{R}$.
- $F_{(k,i)}^k$: External force applied to the beam k at the node i in the local frame.
- $F_{(k,i)}$: External force applied to the beam k at the node i in the global frame.

Each beam k is assumed to be axisymmetric and is defined by its mechanical (E^k, G^k) and geometrical (S_k, L_k, I_k, Io_k) characteristics. The lattice deformation is completely defined by the global force, $F = [F_1 \cdots F_m]^t$ and the node displacement $U = [U_1 \cdots U_m]^t$ expressed in the global frame $\mathcal{R}$.

2.2 Stiffness matrix definition

For simplification reasons, we introduce the total force $\hat{F}_k^k = \left[F_{(k,i)}^k \; F_{(k,j)}^k\right]^t$ applied to the beam k at each extremity and the displacement $\hat{U}_k^k = \left[U_i^k \; U_j^k\right]^t$ of each beam extremity. Hence, the local stiffness matrix of the beam k is defined such as $\hat{F}_k^k = K_k^k.\hat{U}_k^k$ with:

$$K_k^k = \left[\begin{array}{c|c} A_k^k & C_k^k \\ \hline (C_k^k)^t & B_k^k \end{array}\right] \quad (2)$$

where the components of A_k^k, C_k^k, and B_k^k calculated by Euler Bernoulli beam theory are given in Appendix A. The transformation from the global frame $\mathcal{R}$ to the local frame $\mathcal{R}^k$ of the beam k can be expressed thanks to the Euler's angles θ_k and ϕ_k giving the matrix $M_{\mathcal{R}\mathcal{R}^k} = R_y(\frac{\pi}{2} - \phi_k).R_z(\theta_k)$ (Fig. 5). The external forces and the displacement can be easily expressed in the global frame by $U_i = M^*_{\mathcal{R}\mathcal{R}^k}.U_i^k$ and $F_{(k,i)} = M^*_{\mathcal{R}\mathcal{R}^k}.F_i^k$ with :

$$M^*_{\mathcal{R}\mathcal{R}^k} = \left[\begin{array}{c|c} M_{\mathcal{R}\mathcal{R}^k} & 0 \\ \hline 0 & M_{\mathcal{R}\mathcal{R}^k} \end{array}\right] \quad (3)$$

It is thus possible to define the stiffness matrix in the global frame to calculate the relationship $\hat{F}_k = K_k.\hat{U}_k$:

$$K_k = \left[\begin{array}{c|c} M^*_{\mathcal{R}\mathcal{R}^k} & 0 \\ \hline 0 & M^*_{\mathcal{R}\mathcal{R}^k} \end{array}\right].K_k^k.\left[\begin{array}{c|c} (M^*_{\mathcal{R}\mathcal{R}^k})^t & 0 \\ \hline 0 & (M^*_{\mathcal{R}\mathcal{R}^k})^t \end{array}\right] \quad (4)$$

2.3 Energy balance

For each beam k, the deformation energy is defined by $E_k^{def} = \frac{1}{2}.\hat{U}_k^t.K_k.\hat{U}_k$. Hence the total energy of deformation is defined by:

$$E_{tot}^{def} = \sum_{k\in[1,n]} \frac{1}{2}.\hat{U}_k^t.K_k.\hat{U}_k \quad (5)$$

The global stiffness matrix K is calculated by assembling all the stiffness matrices. Therefore, the total energy of deformation becomes:

$$E_{tot}^{def} = \frac{1}{2}.U^t.K.U \quad (6)$$

The solution of the deformation problem consists in the minimization of the total energy. In our case, as the external forces are null the mechanical work $W^{ext} = U^t.F$, so the solution that minimizes the strain energy is the one that minimizes the energy of deformation. The resolution of such a problem is a classic quadratic optimization problem which is solved using Matlab.

The mesh deformation is performed by imposing displacements to the mesh nodes that do not correspond to

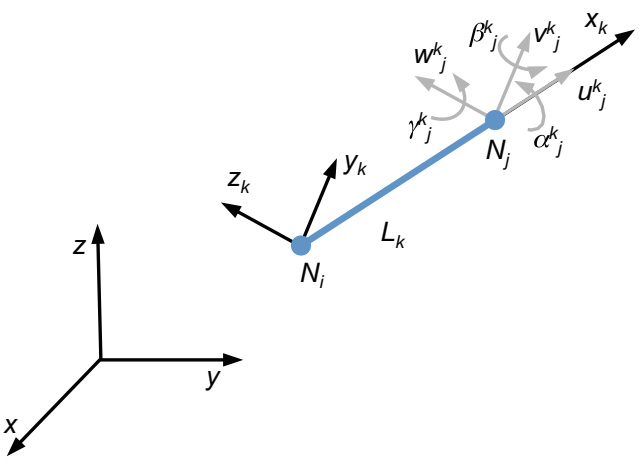

Fig. 4 Beam modeling

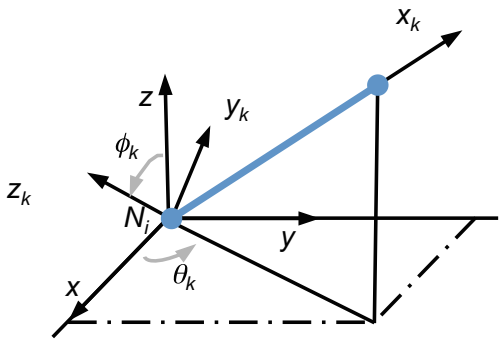

Fig. 5 Frame description

holes and by computing the displacement of the other nodes by minimization of the total energy E_{tot}^{def}. Let us remember here that each displacement includes three translations and three rotations. These 6 degrees of freedom involve both the shape preservation and the continuous evolution of the curvature. On the other hand, mesh deformation calculation can be time-consuming. Indeed, for a classical part (Fig. 2), the mesh includes about 10^5 nodes each having 6 degrees of freedom. The originality of our approach is thus to reduce the minimization problem to zones of interest defined from digitized hole neighborhoods. Finding the holes is thus an essential step in the overall approach as we will see now in more details.

3 General approach

The general approach consists of three main steps (Section 1.2): data registration, hole detection and boundary identification, and mesh deformation. The input data are a nominal mesh and a digitized point cloud corresponding to the scanned data. Finally, the nominal mesh is deformed to match the digitized point cloud which involves the hole filling.

3.1 Data registration

The first step of the approach is a global data registration between the scanned data and the nominal mesh to ensure the correspondence between scanned and nominal features. This step, necessarily performed prior to the mesh deformation enables the point cloud to be close to the nominal mesh. Global registration is achieved using a HT-ICP algorithm [4]. The result is considered satisfactory if the registration error is less than the error imputed to the manufacturing process and/or the digitizing error.

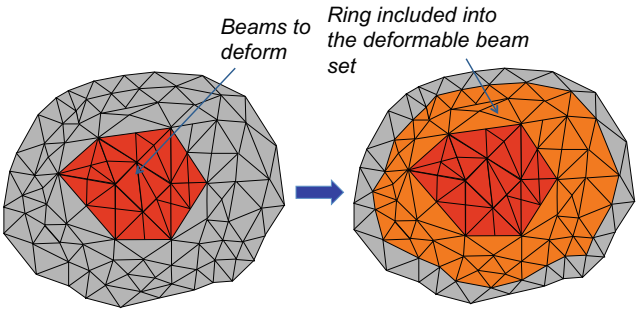

Fig. 7 Boundary definition

3.2 Hole detection and boundary detection

As point clouds obtained from scanning are generally dense and heterogeneous with a lack of continuity [14], finding digitizing holes could be a long and tedious task. To simplify this issue, we propose to take advantage of the initial data registration which leads to a good match between the scanned data and the nominal mesh. Holes are thus identified by considering points that belongs to the nominal mesh for which no equivalent exist in the point cloud.

The main hypothesis here is that the hole dimension is greater than the mesh size. Let us consider a point N of the nominal mesh, and its associated normal vector (Fig. 6). The q closest points to N belonging to the point cloud are identified. A local mesh is built from these q points, and the intersection between the line passing through N and directed along the normal vector is calculated. If the intersection does not exist, as for point N_1 in Fig. 6, the point N is identified as a *hole point*, and the beams linked to this node are classified as *beams to be deformed* (in red in Fig. 6). This hole detection method turns out to be efficient and simple to implement as it is based on the calculation of the vector normal. The facets linked with the considered point are selected, and the normal vector is estimated by calculating the average of the normal vectors of the previously

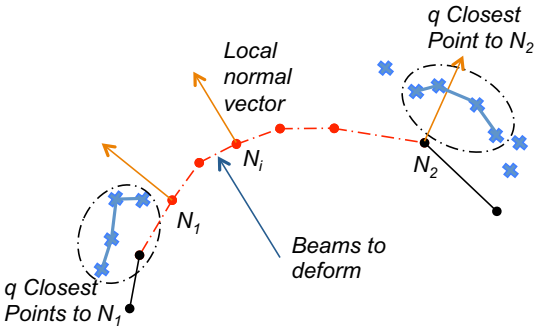

Fig. 6 Hole detection and mesh reduction

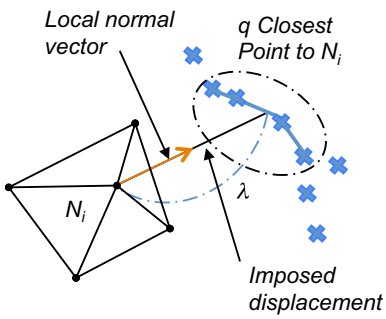

Fig. 8 Displacement computation

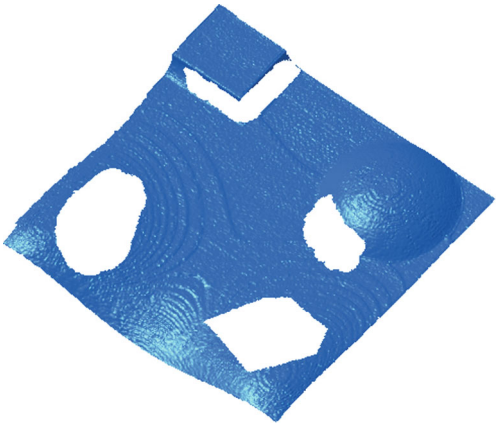

Fig. 9 Digitized point cloud with artificial holes

defined facets. Note that such a method involves the reduction of the mesh to be deformed to a restriction defined by the digitized holes.

3.3 Mesh deformation

To preserve the curvature evolution between the deformed regions and the nominal mesh, it seems relevant to increase the region to be deformed (Fig. 7). Therefore, a ring around the border is defined. The ring's width is defined according to the mesh's size; in this study, the width is equal to three times the mesh's size. The nodes of the nominal mesh that are added to the ring necessarily have their counterpart in the scanned point cloud. For such nodes, a corresponding point can be defined in the scanned point cloud by considering the barycentre of the q nearest points to the given node.

For each node belonging to the border zone (in orange in Fig. 7), the displacement $\mathbf{u}$ is imposed and must

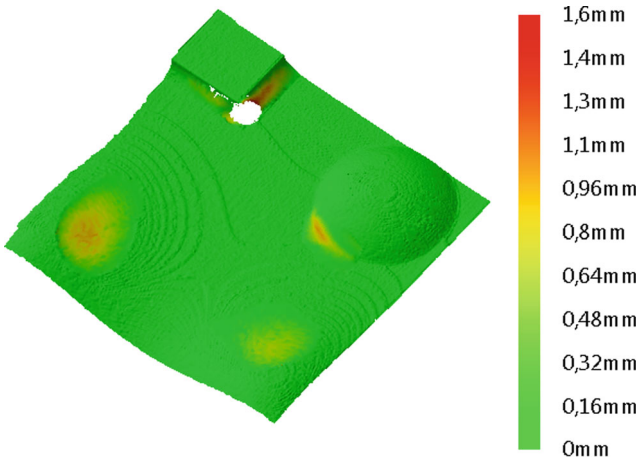

Fig. 10 Deviations between the CAD-filled mesh and the digitized point cloud

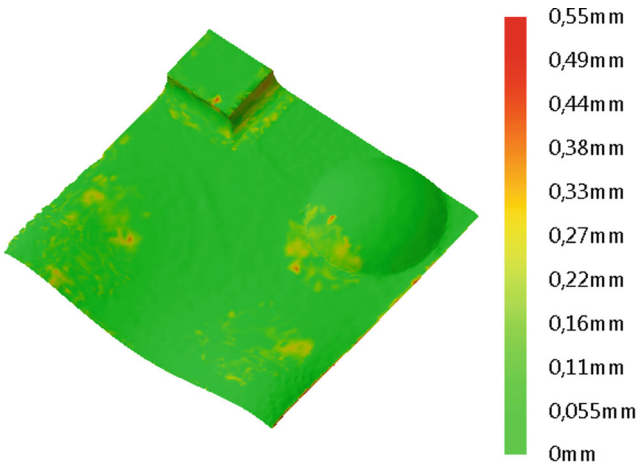

Fig. 11 Deviations between the morphed mesh and the digitized point cloud

be calculated. For such nodes, the intersection between the straight line passing through the point and directed along the vector normal and the mesh created by the q closest points exists (see Section 3.2). The displacement is the one that makes the studied node perfectly matched with its corresponding point: $\mathbf{u}_i = \lambda.\mathbf{n}_i$ with $\mathbf{n}_i$ the normal vector Fig. 8. This defines the generalized displacement of the node i in the global frame that is introduced in the energy minimization problem (Eq. 6):

$$U_i = \left[\lambda.\mathbf{n}_{ix}\ \lambda.\mathbf{n}_{iy}\ \lambda.\mathbf{n}_{iz}\ 0\ 0\ 0\right]^t_{\mathcal{R}}. \tag{7}$$

For other points (in grey in Fig. 7), the displacement is used to reduce the gap between the nominal mesh and the measured points.

The minimization problem thus leads to the deformation of the nominal STL mesh to match the point cloud involving the propagation of the deformation to the digitized holes. Such an approach ensures the preservation of the general shape as the deformation is only applied to the zones of interest around the digitized holes. The management of the curvature continuity at the vicinity of the junction is done thanks to the control of the tree rotations at each node.

Table 2 Results analysis

	Cad filled	Morphing
Maximal deviation	1.6 mm	0.55 mm
Mean Deviation	0.0085 mm	0.044 mm
Standard Deviation	0.067 mm	0.073 mm

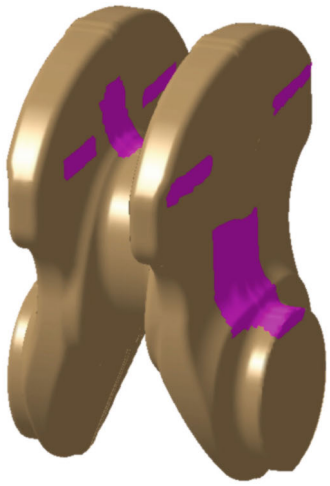

(a) Representation of the nominal mesh

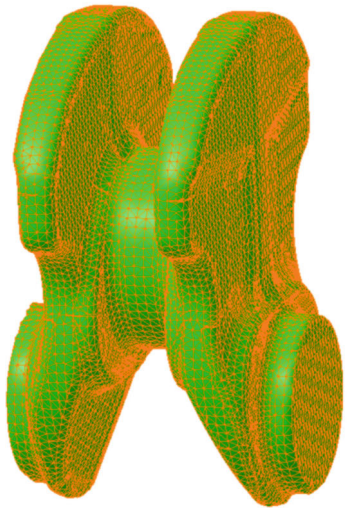

(b) Representation of the morphed mesh

Fig. 12 Representation of the studied part

4 Application

4.1 Study of a sculptured part

The method is applied to a sculptured surface made by 3D printing (ABS plastic part) (Fig. 2) bounded by a 100 x 100 x 15 mm^3 box. The part is scanned using a laser scanner Kreon KZ25 mounted on a coordinate measuring machine (CMM). The manufacturer announces an accuracy of 15 µm. Only one scanner orientation is used during the scanning process in order to reduce the digitizing noise. Under these conditions, the maximal digitizing noise is estimated to be 72 µm [1, 26]. After the scanning is done, artificial holes are added to the actual ones (Fig. 9). To assess our method, the holes are filled using a CAD software (CATIA ©) for which the mesh size is equivalent to that used in the nominal mesh. The mesh that is filled using the aforementioned CAD software is compared to the initial point cloud (Fig. 10). As shown in the figure, the CAD software does not succeed in hole filling as some holes remain unfilled. Furthermore, deviations with the initial mesh can reach up to 1.6 mm which can be penalizing for some applications. Lastly, one can see that curvature continuity is not ensured and so the overall shape is not preserved. The proposed morphing method is applied. Deviations between the morphed mesh and the measured point cloud are displayed in Fig. 11 and a comparison between the CAD-filling approach and our approach is proposed in Table 2. Since the distance between the scanned data and the CAD-filled mesh are identical outside the hole areas, the mean distance and the standard deviation are closed to those obtained with the morphing-based approach. However, the maximal distance is strongly reduced with our algorithm (three times lesser). Furthermore, Fig. 11 clearly highlights smoothing and overall shape preservation.

Nevertheless, high deviations can be observed on the edges of the part. This is likely due to the normal vector calculation, which is deficient when it comes to mesh edges for which there is a lack of information.

Let us see now, the interest of our algorithm for point exploitation, in the particular case of inertia parameter calculation for crankshaft balancing.

Table 3 Computation parameters

Number of nodes of initial mesh	12,718
Number of nodes of restricted mesh	2775
Number of nodes of the scanned mesh	545,007

4.2 Improving crankshaft balancing

This illustration is directly linked with a new method for crankshaft balancing based on non-contact measurement. In this method, once the crankshaft is digitized using a laser-plane scanner, a STL mesh is directly built from the

Table 4 Unbalance in reference planes

Part	Unbalance 1 (g cm)	Unbalance 2 (g cm)
Nominal mesh	261.7	261.5
Morphing	258.9	258.3
Cad filled	253.9	253.8

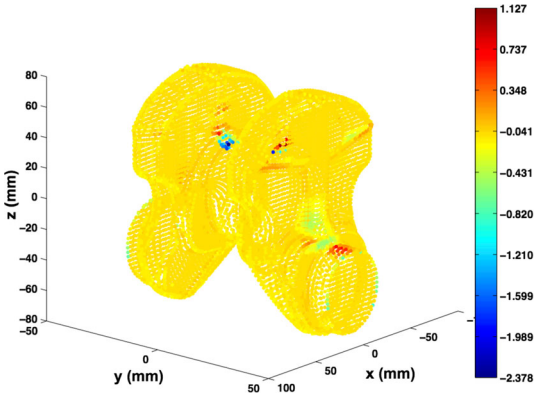

Fig. 13 Deviation (mm) between nominal and morphed crankshaft

digitized points. This mesh, which must define a closed structure, is the support for a voxelisation algorithm [16]. The voxelisation algorithm delivers a 3D structure of voxels, each one being assigned with an elementary mass. The calculation of inertia parameters is carried out considering this 3D structure made of concentrated masses located at the center of each voxel. This method has proven to be efficient for the estimation of the specific unbalances if the digitized point cloud is a complete representation of the shape [26]. Digitized holes can alter unbalance calculation. Indeed, crankshafts are very complex parts, which generally require numerous sensor orientations to access all the surfaces to be measured. As this process is time-consuming, the idea is to limit the number of sensor orientations, and to fill the holes with the morphing-based approach we propose.

For this purpose, the digitizing of the crankshaft is simulated from the CAD model. First, the defects of the manufacturing process are simulated so that the crankshaft has unbalance defects. Rough crankshafts are conventionally obtained by forging. Associated defects are simulated by performing an expansion of 3 % of the nominal CAD model and by carrying out a 0.5 mm shift between the two sections located on both sides of the symmetry plane. To simplify the representation, only a 100 mm portion of the crankshaft is studied (Fig. 12a). Mesh specifications are detailed in Table 3. These defects generate unbalances that are calculated in the two reference planes located on either extremity (Table 4).

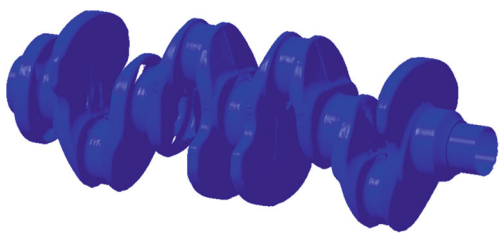

Fig. 14 Digitized crankshaft

Once the defects are simulated, the mesh is calculated from the modified CAD model. To simulate digitizing holes, holes are added to the mesh (represented in purple in Fig. 12a) corresponding to areas that are difficult to scan [26]. Our algorithm is thus applied. Results highlight a mean deviation of 8.7 µm and a standard deviation of 92 µm (Fig. 13). Unbalances are calculated for the morphed mesh. As displayed in Table 4, the values calculated after morphing are close to the actual values. Indeed, the estimated unbalances are determined with an error of less than 1.5 %. To enhance the efficiency of our approach, unbalances obtained using a classical CAD-filling are also calculated and compared to the actual ones. In this case, the error is up to 3 % which could be penalizing for the further balancing operation. Therefore, with the morphed-based approach to fill digitized holes, it is possible to preserve the overall shape of the digitized object, and then, it is also possible to conduct inertia calculations with an error of less than 1.5 % relatively to the actual values.

4.3 Application to digitized data

The method is applied to actual digitized data. The crankshaft is digitized using a structured light sensor (Gom Atos III) positioned thanks to a tripod. Under these conditions, the maximal digitizing noise is estimated at 18 µm [26]. From previous work [11], we know that 50 viewpoints are necessary to reach completeness. However, digitizing holes are present in the point cloud in non-accessible areas (Fig. 14). To clarify the representation, only the *arm* connecting the crankpin to the crank journal and one of the cylinders machined at both extremities are specifically studied (Figs. 15b and 16b).

The *arm* is bounded by a 85 x 40 x 110 mm^3 box. According to the proposed method, the nominal mesh (Fig. 15a) is deformed, and the morphed mesh is displayed in Fig. 15c, d. Point identified as holes (Section 3.2) are represented in red, and points of the border used to impose displacements (Section 3.3) are represented in orange. Despite the complexity of the hole boundary (Fig. 15b) and of the digitizing noise, the mesh morphing leads to a satisfactory result as the shape is clearly preserved, along with the curvature evolution 15d. The morphed mesh can replace the point cloud for further point exploitation. This result highlights the performance of the method for filling actual digitized holes.

Regarding the second part, it consists of a 41 mm diameter and 19 mm length cylinder (Fig. 16a). In this case, the

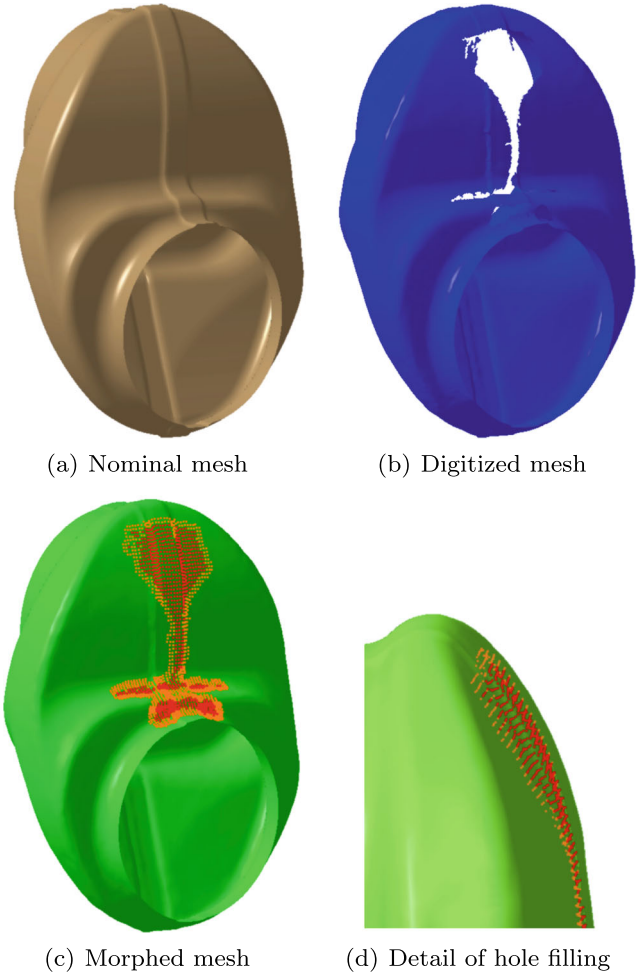

Fig. 15 Representation of studied part of the crankshaft

lack of data corresponds to the top plane (Fig. 16b). As displayed in the figure, only a few points are digitized on the plane surface, which involves that only a few points can be used to define the border of the planar portion. In addition, due to the tangency discontinuity between the plane and the cylinder, digitizing noise is high in this area. As a result, the calculation of the imposed displacements is heavily altered, and the resulting morphed mesh is incorrect (Fig 16c).

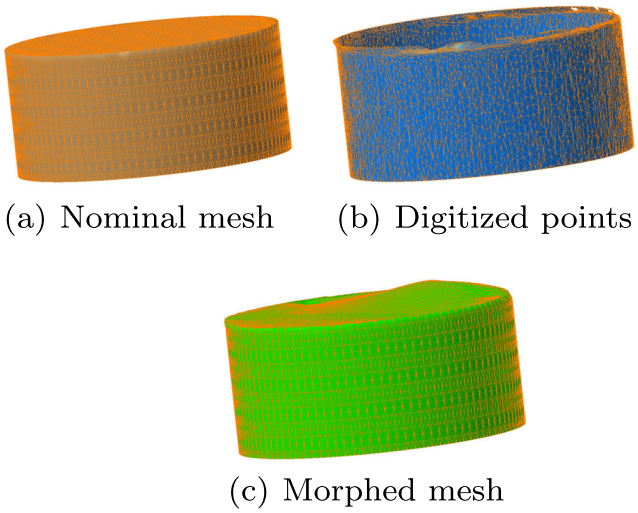

Fig. 16 The studied cylinder

4.4 Discussion

The applications we proposed highlight the relevance of the morphing-based approach based on the CAD model to fill digitizing holes prior to point exploitation. This is clearly illustrated through the crankshaft balancing example. When digitized data are used, although digitized holes present a complex geometry, and despite digitizing noise, the morphed mesh can be calculated. The general shape is preserved and all the holes are filled considering curvature continuity at the junctions. However, the method present some limits. First, the manufacturing process is assumed to be controlled, i.e., the shape of the actual part is not very different from the shape of the nominal part. This is generally the case for machining or additive manufacturing operations as proposed here. In addition, the hole must not cover a complete feature, as it is the case with the top plane of the cylinder. The great lack of points on the surface involves a bad shape prediction. Finally, digitizing noise can be penalizing at the vicinity of the part edges for which the evaluation of the normal vector can be deficient.

5 Conclusion

A complete approach has been presented in this paper for filling holes in point clouds with a priori knowledge of the CAD model. This approach relies on the morphing of the CAD model represented as a mesh according to the minimization of the mechanical energy. The mesh is associated to a beam lattice and, to preserve curvature continuity, all types of solicitations are considered (torsion, bending, and stretching). Hole-filling with shape preservation is particularly essential to facilitate applications such as rapid prototyping, finite element analysis, or inertia calculations as proposed in this paper. To prevent substantial computational time, a method of restriction of the meshes to the digitized hole areas has been developed. This method preserves the curvature connection between the deformed areas and the nominal mesh. As crankshaft balancing using optical means is nowadays a challenging issue, the application of the proposed approach concerns the calculation of unbalances using incomplete simulated digitized data. Using our approach,

in comparison with classical CAD-filling methods, showed a significant decrease in unbalance determination. The relevance of the morphing-based approach based on the CAD model to fill digitizing holes is also illustrated by actual digitized data. The method is efficient when the manufacturing process is controlled and when data are not affected by the digitizing noise (when it remains inferior to the mean value of the sensor noise. The morphed mesh can thus replace the point cloud for further point exploitation. Such a method could also help in the definition of digitizing strategy for complex parts. Indeed, complete digitizing is not necessary anymore when digitizing holes can be accurately filled with shape preservation.

Appendix A: stiffness matrix description

$$K_k^k = \left[\begin{array}{c|c} A_k^k & C_k^k \\ \hline (C_k^k)^t & B_k^k \end{array}\right] \tag{8}$$

$$A_k^k = \begin{bmatrix} \frac{E^k.S^k}{L^k} & 0 & 0 & 0 & 0 & 0 \\ 0 & \frac{12.E^k.I^k}{(L^k)^3} & 0 & 0 & 0 & \frac{6.E^k.I^k}{(L^k)^2} \\ 0 & 0 & \frac{12.E^k.I^k}{(L^k)^3} & 0 & -\frac{6.E^k.I^k}{(L^k)^2} & 0 \\ 0 & 0 & 0 & \frac{G^k.Io^k}{L^k} & 0 & 0 \\ 0 & 0 & -\frac{6.E^k.I^k}{(L^k)^2} & 0 & \frac{4.E^k.I^k}{L^k} & 0 \\ 0 & \frac{6.E^k.I^k}{(L^k)^2} & 0 & 0 & 0 & \frac{4.E^k.I^k}{L^k} \end{bmatrix} \tag{9}$$

$$B_k^k = \begin{bmatrix} \frac{E^k.S^k}{L^k} & 0 & 0 & 0 & 0 & 0 \\ 0 & \frac{12.E^k.I^k}{(L^k)^3} & 0 & 0 & 0 & -\frac{6.E^k.I^k}{(L^k)^2} \\ 0 & 0 & \frac{12.E^k.I^k}{(L^k)^3} & 0 & \frac{6.E^k.I^k}{(L^k)^2} & 0 \\ 0 & 0 & 0 & \frac{G^k.Io^k}{L^k} & 0 & 0 \\ 0 & 0 & \frac{6.E^k.I^k}{(L^k)^2} & 0 & \frac{4.E^k.I^k}{L^k} & 0 \\ 0 & -\frac{6.E^k.I^k}{(L^k)^2} & 0 & 0 & 0 & \frac{4.E^k.I^k}{L^k} \end{bmatrix} \tag{10}$$

$$C_k^k = \begin{bmatrix} -\frac{E^k.S^k}{L^k} & 0 & 0 & 0 & 0 & 0 \\ 0 & -\frac{12.E^k.I^k}{(L^k)^3} & 0 & 0 & 0 & \frac{6.E^k.I^k}{(L^k)^2} \\ 0 & 0 & -\frac{12.E^k.I^k}{(L^k)^3} & 0 & -\frac{6.E^k.I^k}{(L^k)^2} & 0 \\ 0 & 0 & 0 & -\frac{G^k.Io^k}{L^k} & 0 & 0 \\ 0 & 0 & \frac{6.E^k.I^k}{(L^k)^2} & 0 & \frac{2.E^k.I^k}{L^k} & 0 \\ 0 & -\frac{6.E^k.I^k}{(L^k)^2} & 0 & 0 & 0 & \frac{2.E^k.I^k}{L^k} \end{bmatrix} \tag{11}$$

Appendix B: frame transformation description

$$M_{\mathcal{R}\mathcal{R}^k} = \begin{bmatrix} \cos\left(\frac{\pi}{2}-\phi_k\right) & 0 & \sin\left(\frac{\pi}{2}-\phi_k\right) \\ 0 & 1 & 0 \\ -\sin\left(\frac{\pi}{2}-\phi_k\right) & 0 & \cos\left(\frac{\pi}{2}-\phi_k\right) \end{bmatrix} \cdot \begin{bmatrix} \cos(\alpha) & -\sin(\theta_k) & 0 \\ \sin(\theta_k) & \cos(\theta_k) & 0 \\ 0 & 0 & 1 \end{bmatrix} \tag{12}$$

References

1. Audfray N, Mehdi-souzani C, Lartigue C (2012) A novel approach for 3d part inspection using laser-plane sensors. In: 12th CIRP conference on computer aided tolerancing, pp 1–3
2. Bernard A (2005) Virtual engineering: methods and tools. Proc Inst Mech Eng B J Eng Manuf 219:413–421
3. Besl PJ, Kay NDM (1992) A method for registration of 3d shape. IEEE Trans Pattern Anal Mach Intell 14(5)
4. Chen J, Wu X, Wang MY, Li X (2013) 3d shape modeling using a self-developed hand-held 3d laser scanner and an efficient ht-icp point cloud registration algorithm. Opt Laser Technol 45:414–423
5. Choi J, Szymczak A (2009) Fitting solid meshes to animated surfaces using linear elasticity. ACM Trans Graph - TOG 28(1):1–10
6. Derigent W, Chapotot E, Ris G, Remy S, Bernard A (2007) 3d digitizing strategy planning approach based on a cad model. J Comput Inf Sci Eng 7(1):10–19
7. Galantucci LM, Percoco G, Spina R (2003) Evaluation of rapid prototypes obtained from reverse engineering. Proc Inst Mech Eng B J Eng Manuf 217:1543–1552
8. Grassia L, Hraiechb N, Schileoa E, Ansalonia M, Rochetteb M, Vicecontia M (2011) Evaluation of the generality and accuracy of a new mesh morphing procedure for the human femur. Med Eng Phys 33:112–120
9. Jun Y (2005) A piecewise hole filling algorithm in reverse engineering. Comput Aided Des 37(2):263–270
10. Kho Y, Garland M (2005) Sketching mesh deformations. In: Proceedings of the ACM symposium on interactive 3D graphics
11. Lartigue C, Quinsat Y, Mehdi-souzani C, Zuquete-Guarato A, Tabibian S (2014) Voxel-based path planning for 3d scanning of mechanical parts. Comput Aided Des Applic 11(3):220–227
12. Li Z, Meek DS, Wlaton D (2010) Polynomial blending in a mesh hole-filling application. Comput Aided Des 42(4):340–349
13. Martins FAR, Garci-Bermejo J, Casanova EZ, Gonzalez JRP (2005) Automated 3d surface scanning based on cad model, mechatronics. Mechatronics 15:837–857
14. Medhi-Souzani C, Thiebaut F, Lartigue C (2006) Scan planning strategy for a general digitized surface. J Comput Inf Sci Eng 6(4):331–340
15. Panchetti M, Pernot JP, Véron P (2010) Towards recovery of complex shapes in meshes using digital images for reverse engineering applications. Comput Aided Des 42(8):693–707
16. Patil S, Ravi B (2005) Voxel-based representation, display and thickness analysis of intricate shapes. In: 9th International conference on computer aided design and computer graphics
17. Pernot JP, Moraru G, Vron P (2006) Filling holes in meshes using a mechanical model to simulate the curvature variation minimization. Comput Graph 30(6):892–902

18. Soren L, Kjellander J (2008) Path planning for laser scanning with an industrial robot. Robot Auton Syst 56(7):615–624
19. Wang J, Oliveira M (2007) Filling holes on locally smooth surfaces reconstructed from point clouds. Image Vis Comput 25(1):103–113
20. Wang LC, Y-C H (2012) Hole filling of triangular mesh segments using systematic grey prediction. Comput Aided Des 44(12):1182–1189
21. Wang X, Liu X, Lu L, Cao BLJ, Yinf B, Shig X (2012) Automatic hole-filling of cad models with feature preserving, computers and graphics. Comput Graph 36(2):101–110
22. Wu X, Chen J, Wang MY, Li X (2011) Hong-tan based icp registration for partially overlapping range images. VRCAI
23. Zheng SX, Li J, Sun QF (2011) A novel 3d morphing approach for tooth occlusal surface reconstruction. Comput Aided Des 43(3):293–302
24. Zhou X, Su Z, Liu X (2010) A novel energy-based method for mesh deformation. In: International conference on educational and information technology, pp 153–156
25. Zhu L, Barhak J, Srivatsan V, Katzr R (2007) Efficient registration for precision inspection of free-form surfaces. Int J Adv Manuf Technol 32:505–515
26. Zuquete-Guarato A, Mehdi-souzani C, Quinsat Y, Lartigue C, Sabri L (2012) Towards a new concept of in-line crankshaft balancing by contact less measurement: process for selecting the best digitizing system. In: 11th Biennial conference on engineering systems and design analysis